

Gravitational wave forest from string axiverse

Naoya Kitajima^a, Jiro Soda^b, Yuko Urakawa^{a,c}

a. Department of Physics and Astrophysics, Nagoya University, Chikusa, Nagoya 464-8602, Japan

b. Department of Physics, Kobe university, Kobe 657-8501, Japan

c. Institut de Ciències del Cosmos, Universitat de Barcelona, Martí i Franques 1 08028, Barcelona, Spain

ABSTRACT: Axions predicted in string theory may have a scalar potential which has a much shallower potential region than the conventional cosine potential. We first show that axions which were located at such shallow potential regions generically undergo prominent resonance instabilities: the well-known narrow resonance and/or the flapping resonance, which has not been well investigated. We also study non-linear dynamics of axions caused by these resonance instabilities based on lattice simulation. We find that string axions in various mass ranges generate gravitational waves (GWs) with peaks at various frequencies determined by the mass scales, dubbed the GW forest. This may allow us to explore string axiverse through future multi-frequency GW observations. We also investigate GWs produced by the axion which accounts for present dark matter component.

KEYWORDS: string axiverse, flapping resonance, GW forest.

Contents

1. Introduction	1
2. Axion dynamics with plateau potential	2
2.1 Axion potential with a plateau region	3
2.2 Plateau potential and delayed oscillation	4
2.3 Instability of inhomogeneous modes	7
2.3.1 Tachyonic instability: Phase 1	8
2.3.2 Flapping resonance: Phase 2	8
2.3.3 Narrow resonance: Phase 3	10
2.4 Overall evolution in linear regime	12
3. Lattice simulation	13
3.1 Nonlinear dynamics of the axion	13
3.2 Oscillon formation	15
4. GW emission	16
4.1 GW spectrum	17
4.2 GW forest	19
4.3 GWs from axion dark matter	21
5. Conclusion	23

1. Introduction

After the first direct detection of gravitational waves (GWs) [1], we are now in an era of GWs. An important lesson from the history of astronomy with electromagnetic waves is that multi-frequency observations of GWs become important. Roughly speaking, there are three categories of GW sources: astrophysical, cosmological, and primordial sources. GWs from astrophysical sources in the kHz band have been detected by GW interferometers. It is now compelling to discover the primordial GWs from inflation by measuring B-mode polarization of cosmic microwave background [2, 3]. In addition to these sources, there are several cosmological GW production processes. For example, parametric amplification of scalar fields during reheating after inflation, cosmic strings, bubbles produced at the first order phase transition belong to this category. As a preparation for the forthcoming era of multi-frequency GW observations by e.g. space-based [4] and ground-based detectors [5] and pulsar timing observations [6], it is worth exploring other cosmological sources of GWs with a wide range of frequencies.

From a theoretical viewpoint, the GWs from astrophysical sources have brought us the information on strong gravity, black hole physics, nuclear physics, star formation, and so on. A detection of the primordial GWs, which will be a first evidence of quantized gravitons, will tell us the energy scale of inflation. GWs from bubbles and cosmic strings provide us the information on cosmological phase transitions. Along this line, it is natural to ask if we can probe fundamental physics through GW observations.

String theory predicts the presence of six dimensional internal space in addition to our four dimensional world. The extra dimensions must be compactified and the compactification of the internal space yields various moduli fields, including axion fields in the four dimensional low energy effective field theory [7,8]. Intriguingly, according to string theory, the mass spectrum of axions can be logarithmically flat. Hence the axions with various masses are ubiquitous in the Universe, which is named string axiverse [9]. It is, therefore, worth exploring imprints of string axiverse in the history of the Universe by means of GWs.

In the previous paper [10], two of the authors initiated a study on GW production from string axiverse to probe the string compactification. It has been suggested that the scalar potential of a string axion may be much shallower than the conventional cosine potential away from the potential minimum [11,12]. When it was located at the shallow potential region before it commences to oscillate, the succeeding dynamics becomes drastically different from the one for an axion with the cosine potential. In fact, such an axion generically undergoes various instabilities after the onset of oscillation. In Ref. [10], it was suggested that these instabilities can lead to a detectable emission of GWs. In this paper, we will investigate this possibility in more detail based on lattice simulation.

The frequency of the emitted GWs is determined by the mass scale of the axion. Historically, an emission of GWs triggered by a coherently oscillating scalar field has been vastly studied in the context of reheating after inflation [13–16]. In this case, frequencies of emitted GWs are typically around 1 GHz [17]. In contrast, string axions with various mass scales lead to GW emissions with various frequency range. These GWs can be a target of multi-frequency GW observations, providing a new window to probe string axiverse, dubbed GW forest.

The paper is organized as follows. In section 2, first we briefly summarize the motivations to consider an axion with a plateau potential, clarifying our definition of the plateau. Then, we discuss different types of instabilities based on linear analysis. In section 3, we investigate the nonlinear dynamics of the axion with lattice simulation, showing that as a consequence of efficient resonance instabilities, clumps of oscillating scalar fields, so-called oscillons, are formed. In section 4, we study that resonance instabilities lead to a copious emission of GWs. We also study the GWs from the axion which survives until now as dark matter. The final section is devoted to the conclusion.

2. Axion dynamics with plateau potential

In this section, we discuss the dynamics of an axion which was initially located at a plateau region in the scalar potential. In this case, the time evolution of the axion becomes drastically different from the one for axions with the conventional cosine potential. We show

that after the axion starts to oscillate, various instabilities set in, clarifying qualitative differences from axions with the cosine potential. These instabilities lead to the highly inhomogeneous spatial distribution of the axion field even if the axion was initially almost homogeneous.

2.1 Axion potential with a plateau region

Axions are conventionally assumed to have the cosine-type potential, given by

$$V(\phi) = \Lambda^4 \left[1 - \cos \left(\frac{\phi}{f} \right) \right], \quad (2.1)$$

where f is the axion decay constant and Λ is the dynamical scale. The axion mass m is given by $m = \Lambda^2/f$. This potential was derived under the dilute instanton gas approximation.

The dilute gas approximation can be broken down, e.g., when the axion is coupled with pure Yang-Mills gauge fields which are strongly coupled. Witten pointed out this possibility by considering an $SU(N)$ gauge theory in large N limit [18, 19]. More recently, the scalar potential of an axion which interacts with an $SU(N)$ gauge field in the large N limit was considered in the context of axion inflation in Ref. [20]. The axion inflation model where the potential of the axion was generated through the dynamics of a pure Yang-Mills gauge theory, was dubbed as *Pure natural inflation* [12]. There, the potential possesses the multi-branch structure, where different branches are obtained by changing ϕ to $\phi + 2\pi n f$ with an integer n . As was argued in Refs. [12, 21], the potential of ϕ in a single branch is typically given in the form:

$$V(\phi) = M^4 \left[1 - \frac{1}{(1 + (\phi/F)^2)^\beta} \right] \quad (\beta > 0) \quad (2.2)$$

with $M \sim N\Lambda$ and $F \propto Nf$. For $\phi/F \ll 1$, this potential is well approximated by the quadratic potential, while for $\phi/F \gtrsim 1$, the potential becomes more flattened and asymptotes to M^4 (there is a caveat for the potential analysis in this region [12, 21]). The potential in the single branch does not preserve the symmetry under $\phi \rightarrow \phi + 2\pi f$, while the periodic symmetry is recovered for the true vacuum energy, which is determined by the minimum values among the different branches [12, 20, 21]. As shown in Refs. [12, 21], for small values of F , the prediction in pure natural inflation becomes compatible with the constraint from Planck 15 [22]. (See also Refs. [23, 24].)

In general, the scalar potential of an axion predicted in string theory acquires multiple cosine terms through non-perturbative effects. A linear combination of several cosine terms can exhibit a wider shallow potential region than the one for a single cosine potential as is discussed, e.g., in multi-natural inflation model [25, 26].

Alternatively, in case the axion has a non-canonical kinetic term or the axion is non-minimally coupled with gravity, the scalar potential can get flattened after the canonical normalization. Therefore, even if the potential of the axion is given by the conventional cosine form, the scalar potential can have a plateau region after the canonical normalization. In Refs. [27–29], it was shown that models of this class, dubbed as α -attractors, rather generically have similar potential structures such as $f(\tanh \phi/\sqrt{6\alpha})$ (see also Ref. [30] for

an earlier study). These potentials typically exhibit flat plateaus for $\phi > \sqrt{6\alpha}$. Notice that in these arguments, the field ϕ appears as a real part of a modulus field and is not an axion.

Along this line, we investigate the dynamics of an axion with a shallow region in the scalar potential and phenomenological consequences. In this paper, we neglect contributions of the axion to the geometry, focusing on the case where the axion starts to oscillate when it was a subdominant component of the universe. Then, introducing a normalized potential $\tilde{V}(\tilde{\phi})$ defined as

$$V(\phi) = (mf)^2 \tilde{V}(\tilde{\phi}), \quad \tilde{\phi} \equiv \frac{\phi}{f}, \quad (2.3)$$

we can express the Klein-Gordon equation in a spatially flat FRW universe as

$$\frac{d^2}{d\tilde{t}^2} \tilde{\phi} + 3 \frac{H}{m} \frac{d}{d\tilde{t}} \tilde{\phi} + \frac{\partial_{\tilde{\mathbf{x}}}^2}{a^2} \tilde{\phi} + \tilde{V}_{\tilde{\phi}} = 0, \quad (2.4)$$

with $\tilde{t} \equiv mt$ and $\tilde{\mathbf{x}} = m\mathbf{x}$. Here, t is the cosmic time, H is the Hubble parameter, and $\tilde{V}_{\tilde{\phi}} \equiv d\tilde{V}/d\tilde{\phi}$. The parameter f corresponds to the decay constant for the conventional cosine potential with $\tilde{V} = 1 - \cos \tilde{\phi}$. For $a \propto t^p$, we can express the Hubble parameter normalized by m as $H/m = p/\tilde{t}$. Notice that the axion's dynamics in a fixed geometry becomes scale free, being independent of the parameters f and m . In contrast, when the axion dominates the universe and the geometry is determined by the axion, the axion's dynamics becomes rather different, depending on f/M_{P} [31], where M_{P} denotes the Planck scale.

2.2 Plateau potential and delayed oscillation

Next, we consider the time evolution of the background homogeneous mode. Likewise a time evolution of an inflaton, at early times when the Hubble friction is large enough, the axion slowly rolls down the potential, behaving as a cosmological constant. When the Hubble parameter decreases to a certain value, H_{osc} , the axion starts to oscillate. For the quadratic potential $V = (m\phi)^2/2$, the Hubble parameter at the onset of the oscillation is given by $H_{\text{osc}} \simeq m$. Meanwhile, for a scalar potential which is shallower than the quadratic form, H_{osc} becomes smaller than m .

To evaluate H_{osc}/m , in general, we need a numerical analysis. However, we can understand that the onset of the oscillation indeed delays for a shallower potential also from a heuristic argument. In the absence of the cosmic expansion, the Klein-Gordon equation for the homogeneous mode is given by $d^2\tilde{\phi}/(d\tilde{t}^2) + \tilde{V}_{\tilde{\phi}} = 0$ and the time scale of the potential driven motion is roughly estimated as $\tilde{t} = mt \simeq \sqrt{|\tilde{\phi}/\tilde{V}_{\tilde{\phi}}|}$. In an expanding universe, the axion commences to oscillate, roughly when the time scale of the potential driven motion becomes comparable to the one of the cosmic expansion, m/H . Therefore, when the axion was initially situated at a potential region with $|\tilde{V}_{\tilde{\phi}}/\tilde{\phi}| < 1$, i.e., at a potential region which is shallower than $\tilde{\phi}^2$, the oscillation does not start yet at $H \simeq m$ and H_{osc}/m becomes smaller than 1, indicating a delayed commencement of the oscillation.

In this paper, to address the situations discussed in the previous subsection, we consider a scalar potential which satisfies

- i) $\tilde{V}(\tilde{\phi}) \rightarrow \tilde{\phi}^2/2$ in the limit $\tilde{\phi} \rightarrow 0$,
- ii) $|\tilde{V}_{\tilde{\phi}}/\tilde{\phi}| \ll 1$ for $|\tilde{\phi}| > 1$.

By a plateau region, we mean a potential region which satisfies the second condition. Most of the properties which will be discussed in this paper follow only from these two conditions. Hence, our discussion can apply to a general scalar field whose potential fulfills the above two conditions, not only to an axion. When we consider axions, we additionally require Z_2 symmetry of the scalar potential, since axions are pseudo scalar fields. When the axion was initially located at a plateau region, since the initial velocity decays immediately and $\tilde{\phi}$ stays almost constant until the onset of the oscillation, evaluating $\tilde{V}_{\tilde{\phi}}/\tilde{\phi}$ with an initial value $\tilde{\phi}_i$, we obtain

$$\frac{H_{\text{osc}}}{m} \simeq \sqrt{\left| \frac{\tilde{V}_{\tilde{\phi}}(\tilde{\phi}_i)}{\tilde{\phi}_i} \right|} \ll 1, \quad (2.5)$$

indicating a significant delay.

Notice that the onset of the oscillation is delayed, as far as the axion stays in a potential region with $|\tilde{V}_{\tilde{\phi}}/\tilde{\phi}| < 1$ sufficiently long in the time scale of the cosmic expansion, even if \tilde{V} does not have an extensive plateau region as is required by the condition ii). For instance, when the axion is initially located around the potential maximum of the cosine potential $\tilde{V} = 1 - \cos \tilde{\phi}$, i.e., at $\tilde{\phi}_i \simeq \pi$, we obtain

$$\frac{\tilde{V}_{\tilde{\phi}}(\tilde{\phi}_i)}{\tilde{\phi}_i} = \frac{\sin \tilde{\phi}_i}{\tilde{\phi}_i} \simeq 0.$$

Meanwhile, the variation of $\tilde{V}_{\tilde{\phi}}/\tilde{\phi}$ in one Hubble time is given by

$$\frac{m}{H} \frac{d}{d(mt)} \frac{\tilde{V}_{\tilde{\phi}}(\tilde{\phi})}{\tilde{\phi}} \Big|_{\tilde{t}=\tilde{t}_i} \simeq -\frac{1}{\pi} \frac{m}{H_i} \frac{d\tilde{\phi}_i}{d\tilde{t}_i}.$$

Therefore, in contrast to the plateau potential, for a significant delay to take place in the cosine potential, the initial velocity $d\tilde{\phi}_i/d\tilde{t}_i$ should be tuned to be a small amplitude. (See Refs. [32, 33] for a time evolution of axion dark matter with the cosine potential under the fine-tuned initial condition.)

In a plateau region which satisfies the condition ii), the curvature of the potential $\tilde{V}_{\tilde{\phi}\tilde{\phi}} \equiv d^2\tilde{V}/d\tilde{\phi}^2$ takes a negative value. Meanwhile, in the limit $\tilde{\phi} \rightarrow 0$, $\tilde{V}_{\tilde{\phi}\tilde{\phi}}$ approaches to 1. Therefore, a potential $\tilde{V}(\tilde{\phi})$ which fulfills the two properties i) and ii) generically has inflection points at $\tilde{\phi} = \pm\tilde{\phi}_c$ with $|\tilde{\phi}_c| = \mathcal{O}(1)$. When the axion was initially located at the plateau region with $|\tilde{\phi}| \gg |\tilde{\phi}_c|$, the subsequent time evolution can be divided into the following phases, depending on the value of the potential curvature $\tilde{V}_{\tilde{\phi}\tilde{\phi}}$:

Phase 1. Rolling down the plateau region with $\tilde{V}_{\tilde{\phi}\tilde{\phi}} < 0$

Phase 2. Oscillation between $\tilde{V}_{\tilde{\phi}\tilde{\phi}} < 0$ and $\tilde{V}_{\tilde{\phi}\tilde{\phi}} > 0$

Phase 3. Oscillation in $0 \leq \tilde{V}_{\tilde{\phi}\tilde{\phi}} \leq 1$

Phase 4. Harmonic oscillation with $\tilde{V}_{\tilde{\phi}\tilde{\phi}} \simeq 1$

In most of the time during the phase 1, the axion slowly rolls down the potential. During the phase 2, 3, and 4, the axion coherently oscillates and in particular during the phase 2 and 3, the oscillation is not yet settled down to the harmonic oscillation.

In the phase 1, 2, and 3, different types of instabilities set in. In the next subsection, we will show that when the onset of the oscillation is delayed, the instabilities during the phase 2 and 3 persist rather long. In the phase 4, the self-interaction of the axion ceases to exist and the axion undergoes the harmonic oscillation, behaving as a dust component.

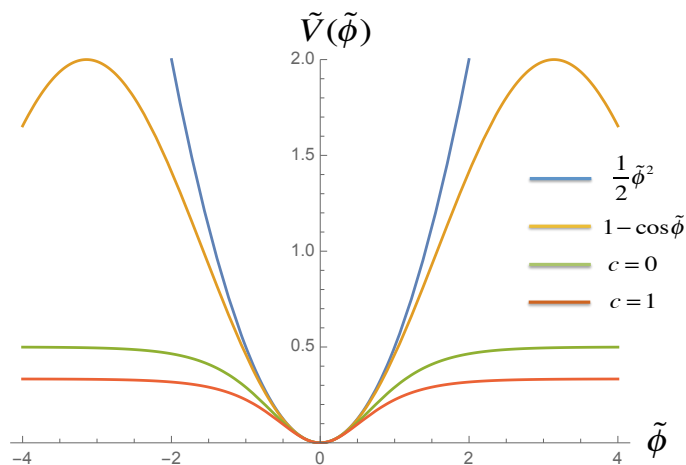


Figure 1: The plot shows the quadratic potential, the cosine potential, and the α attractor type potential for $c = 0, 1$.

As a specific example of the potential which fulfills the above two conditions, here let us consider an α attractor type potential [27–29] given by

$$\tilde{V}(\tilde{\phi}) = \frac{1}{2} \frac{(\tanh \tilde{\phi})^2}{1 + c(\tanh \tilde{\phi})^2} \quad (2.6)$$

with c being a positive numerical constant. The potential form of Eq. (2.6) is shown in Fig.1 for $c = 0, 1$ together with the quadratic potential and the cosine type potential. We numerically solved the background dynamics for various sets of the parameters $(c, \tilde{\phi}_i)$ under the slow-roll initial condition during radiation domination. Fig. 2 shows the time evolution of $\tilde{\phi}$ (left) and $\tilde{V}_{\tilde{\phi}\tilde{\phi}}$ (right) for $(c, \tilde{\phi}_i) = (0, 3), (1, 3), (5, 3)$ (the horizontal axis is $\tilde{t} \equiv mt$). The left panel of Fig. 2 shows the delayed onset of oscillation, i.e. $m/H_{\text{osc}} = 2\tilde{t}_{\text{osc}} \gg 1$, and it becomes more significant for larger c . Notice that while the phase 2 finishes after several oscillations for $c = 0$, it continues much longer for $c = 5$. Since the Hubble friction is no longer important during the oscillation period, $\tilde{V}_{\tilde{\phi}\tilde{\phi}}$ significantly deviates from 1 over many periods of the oscillation.

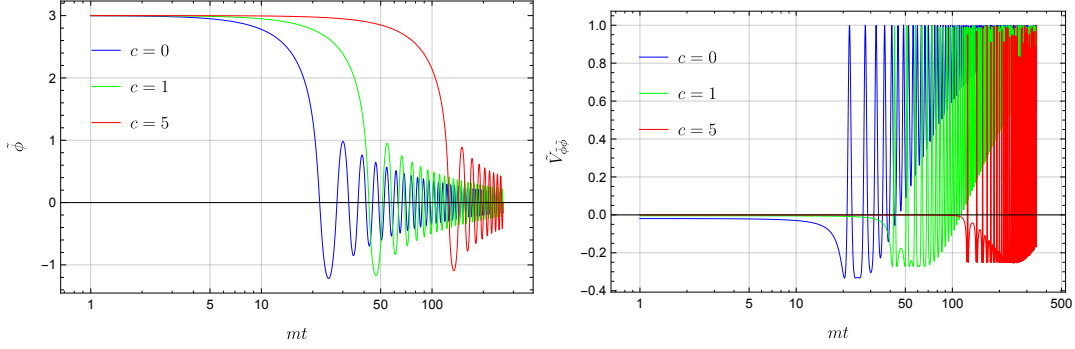


Figure 2: The left panel shows the time evolution of $\tilde{\phi}$ and the right one shows the time evolution of $\tilde{V}_{\tilde{\phi}\tilde{\phi}}$ for the α attractor potential. We have taken $\tilde{\phi}_i = 3$ and $c = 0$ (blue), 1 (green), 5 (red).

2.3 Instability of inhomogeneous modes

In this subsection, we study the dynamics of inhomogeneous modes of the axion during the phase 1, 2, and 3 based on linear analysis. Perturbing Eq. (2.4), we obtain the evolution equation for Fourier modes of the dimensionless linear perturbation $\delta\tilde{\phi}_k (= \delta\phi_k/f)$ as

$$\frac{d^2}{dt^2}\delta\tilde{\phi}_k + 3\frac{H}{m}\frac{d}{dt}\delta\tilde{\phi}_k + \left(\frac{k}{am}\right)^2\delta\tilde{\phi}_k + \tilde{V}_{\tilde{\phi}\tilde{\phi}}\delta\tilde{\phi}_k = 0, \quad (2.7)$$

where we neglected the metric perturbations. This can be verified when the self-interaction of the axion dominates the gravitational interaction, which is the case of our interest.

For a computational simplicity, let us introduce another variable as $\varphi_k = a^{3/2}\delta\tilde{\phi}_k$. The equation of motion (2.7) is now recast into

$$\frac{d^2}{dt^2}\varphi_k + \omega_k^2\varphi_k = 0 \quad (2.8)$$

with

$$\omega_k^2 \equiv \left(\frac{k}{am}\right)^2 + \tilde{V}_{\tilde{\phi}\tilde{\phi}} - \frac{9}{4}\left(\frac{H}{m}\right)^2 - \frac{3}{2}\frac{\dot{H}}{m^2} \simeq \left(\frac{k}{am}\right)^2 + \tilde{V}_{\tilde{\phi}\tilde{\phi}}. \quad (2.9)$$

Here and hereafter, focusing on the case with the delayed oscillation, we drop the terms which are suppressed for $H/m \ll 1$.

Eq. (2.8) can be regarded as one dimensional kinematics governed by the quadratic potential

$$\mathcal{V}_k \equiv \frac{1}{2}\omega_k^2\varphi_k^2 \simeq \frac{1}{2}\left[\left(\frac{k}{am}\right)^2 + \tilde{V}_{\tilde{\phi}\tilde{\phi}}\right]\varphi_k^2. \quad (2.10)$$

The first term in the right hand side always acts as a restoring force, which drives φ_k towards the origin. On the other hand, the potential driven force, the second term, acts more non-trivially, since it flips the signature at the inflection points. In the previous subsection, we divided the time evolution of the homogeneous mode into four different phases, depending on the value of $\tilde{V}_{\tilde{\phi}\tilde{\phi}}$. In the following, we will show that inhomogeneous modes undergo different types of instabilities in different phases.

2.3.1 Tachyonic instability: Phase 1

During the phase 1, (the homogeneous mode of) the axion rolls down the plateau region, where $\tilde{V}_{\tilde{\phi}\tilde{\phi}}$ takes a negative value. During this period, ω_k^2 takes a negative value for the low- k modes with

$$\frac{k}{am} < \sqrt{|\tilde{V}_{\tilde{\phi}\tilde{\phi}}|}, \quad (2.11)$$

and these modes grow exponentially. In particular, the growth rate of the modes with $k/(am) \ll \sqrt{|\tilde{V}_{\tilde{\phi}\tilde{\phi}}|}$ become independent of k . Such a tachyonic instability occurs also during the reheating process [34].

2.3.2 Flapping resonance: Phase 2

In this phase, the axion goes back and forth between the regions with $\tilde{V}_{\tilde{\phi}\tilde{\phi}} < 0$ and $\tilde{V}_{\tilde{\phi}\tilde{\phi}} > 0$. During the term when $\tilde{V}_{\tilde{\phi}\tilde{\phi}}$ takes a negative value, the low- k modes with Eq. (2.11) can be enhanced by the tachyonic instability. However, the tachyonic instability is not sustainable, because $\tilde{V}_{\tilde{\phi}\tilde{\phi}}$ flips the signature when the oscillating homogeneous mode crosses the inflection point(s). Because of that, ω_k^2 also flips the signature for the low- k modes, letting the potential \mathcal{V} flaps during each oscillation of the homogeneous mode. In particular, every time ω_k^2 changes the signature, the adiabatic condition is significantly violated, taking a large value of $|\frac{d\omega_k}{dt}/\omega_k^2|$. The violation of the adiabatic condition is the crucial difference between the instability in the phase 2 and the instabilities in the phase 1 and 3.

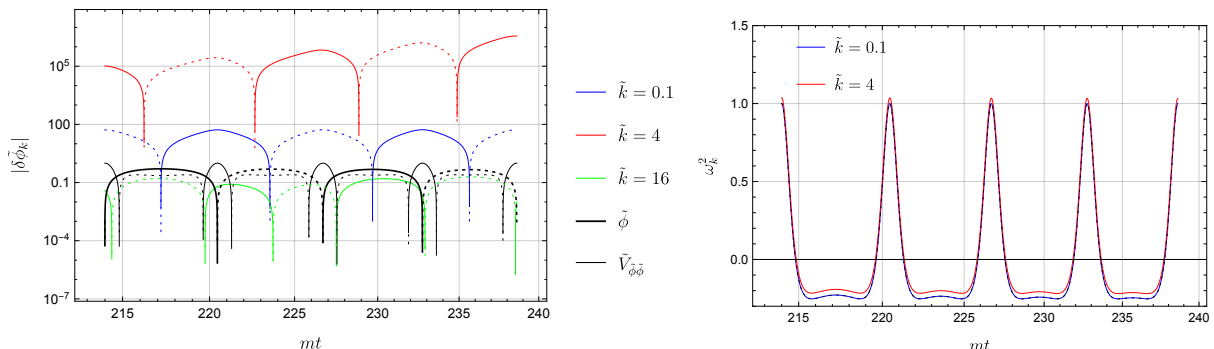


Figure 3: The left panel shows the time evolution of $\delta\tilde{\phi}_k$ for different wave numbers $\tilde{k} = k/(a_{H=m}m) = 0.1$ (blue), $\tilde{k} = 4$ (red), and $\tilde{k} = 16$ (green) during radiation domination. Here, we consider the α attractor potential with $c = 5$ under the slow-roll initial condition with $\tilde{\phi}_i = 3$. We also showed the time evolution of $\tilde{\phi}$ (black thicker) and $\tilde{V}_{\tilde{\phi}\tilde{\phi}}$ (black thinner). We distinguished positive values and negative values, using solid lines for the former and dotted lines for the latter. The right panel shows the time evolution of ω_k^2 for $\tilde{k} = 0.1$ (blue) and $\tilde{k} = 4$ (red). The black dotted line shows $\omega_{k=0}^2 = \tilde{V}_{\tilde{\phi}\tilde{\phi}}$, which coincides with the one for $\tilde{k} = 0.1$.

For the conventional broad resonance, inhomogeneous modes are largely enhanced at the moment when the adiabatic condition is violated. By contrast, for the instability in the phase 2, the enhancement takes place when ω_k^2 takes negative values and finishes, when

it turns to be positive, violating the adiabatic condition. This can be seen in Fig. 3, which shows a typical time evolution of $\delta\tilde{\phi}_k$ (left) and ω_k^2 (right) during this phase obtained by numerical calculation. Here, we considered the α attractor type potential (2.6) with $c = 5$, choosing the initial condition $\tilde{\phi}_i = 3$. For a reference, we also plotted the time evolution of the background mode, $\tilde{\phi}$ and $\tilde{V}_{\tilde{\phi}\tilde{\phi}}$. The three different modes with $\tilde{k} \equiv k/(a_{H=m}m) = 0.1, 4, 16$ evolve in a different way. In the following, we set the scale factor at $H = m$, $a_{H=m}$, to unity. Since ω_k^2 with $\tilde{k} = 16$ is always positive (during the time period plotted in Fig. 3), this mode simply oscillates without tachyonic growth. Meanwhile, ω_k^2 becomes negative during each oscillation of $\tilde{\phi}$ for both $\tilde{k} = 0.1$ and $\tilde{k} = 4$. However, only the mildly low- k mode, $\tilde{k} = 4$, manages to grow after two oscillations of $\tilde{\phi}$ plotted in Fig. 3.

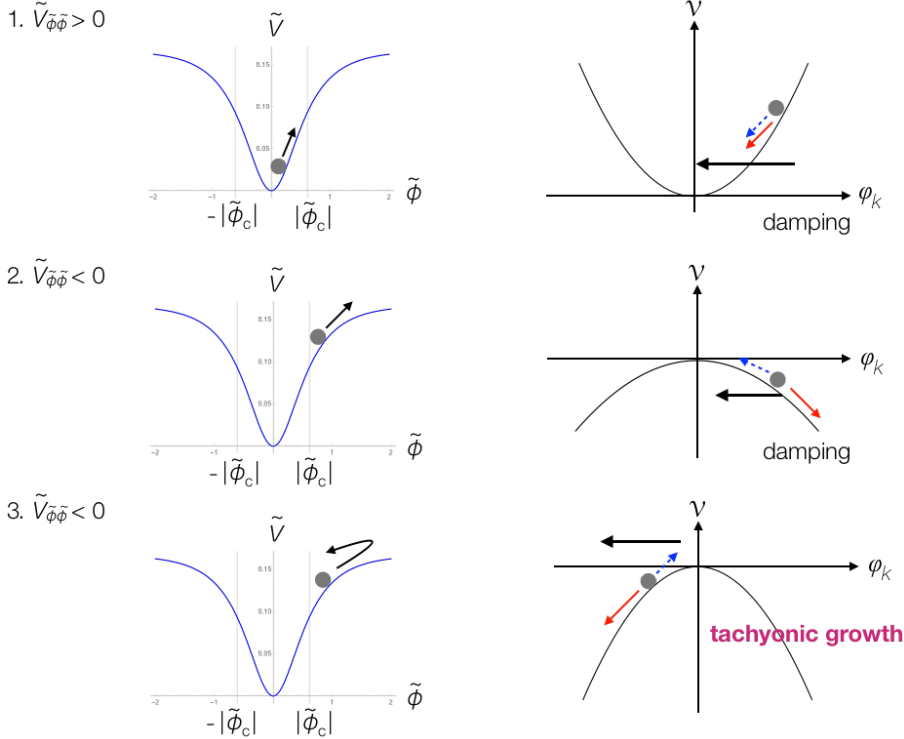


Figure 4: This figure gives a schematic image of how the low- k modes evolve during the phase 2. The blue dotted arrow shows the “permanent” restoring force, determined by the first term in (2.10), and the red arrow denotes the potential driven force. The black thicker arrow shows the velocity, i.e., the direction of the motion, of φ_k .

Figure 4 illustrates the reason for this. The blue dotted arrow denotes the restoring force, determined by the first term in (2.10), and the red arrow denotes the potential driven force, which changes the signature for the flapping potential. In the first layer of Fig. 4, which corresponds to the left-most moment in Fig. 3, since the homogeneous mode is within the inflection points, taking $\tilde{V}_{\tilde{\phi}\tilde{\phi}} > 0$, the potential driven force also acts as an additional restoring force, which is independent of the wavenumber and drives φ_k towards the origin. As depicted in the second layer in Fig. 4, once the homogeneous mode passes beyond the

inflection point, the flapping potential immediately becomes convex. During this term, φ_k climbs the potential hill, consuming the kinetic energy obtained in the previous stage. Once φ_k crosses the origin, as depicted in the third layer, φ_k goes down the potential hill, increasing the amplitude through the tachyonic instability. The tachyonic growth lasts, until the zero mode comes within the inflection points and the curvature of \mathcal{V}_k , given by ω_k^2 , turns to be positive as in the first layer of Fig. 4. The flow of these steps repeats during the phase 2, where $\tilde{V}_{\tilde{\phi}\tilde{\phi}}$ flips the signature during each oscillation of the homogeneous mode.

The key to understand the difference between the two modes $\tilde{k} = 0.1$ and $\tilde{k} = 4$ is in the presence of the second layer stage, i.e., the amplitude of φ_k does not start to grow immediately after $\tilde{V}_{\tilde{\phi}\tilde{\phi}}$ becomes negative. Reducing the duration of this stage leads to a net growth, acquiring a longer time for the tachyonic growth in the third layer stage. Notice that in the second layer stage, the potential driven force acts as a resistive force against the motion of φ_k towards the origin, while the “permanent” restoring force, which is proportional to $(k/am)^2$, supports the motion towards the origin. Because of that, as shown in Fig. 3, (the amplitude of) the mode $\tilde{k} = 4$ turns to grow prior to $\tilde{k} = 0.1$ after $\tilde{V}_{\tilde{\phi}\tilde{\phi}}$ becomes negative. For $\tilde{k} = 0.1$, since the growth during the third layer stage is canceled by the decay in the first layer and the second layer stages, there is no net growth.

We dub the instability in the phase 2, which resonates with the flapping ω_k^2 or \mathcal{V}_k , *the flapping resonance instability*, distinguishing it from the usual broad resonance instability and also from the usual tachyonic instability. Unlike the usual broad resonance instability and the tachyonic instability, the flapping resonance generates a peak at $k \neq 0$ in the spectrum. This is because the tachyonic instability takes place only for low- k modes and a larger k mode can be enhanced in a longer time among these low- k modes. Therefore, the peak wavenumber generated by the flapping resonance instability is roughly estimated by the maximum wavenumber among those which undergo the tachyonic instability as

$$\frac{k_{\text{peak}}}{a_{\text{res}}m} \simeq \sqrt{|\tilde{V}_{\tilde{\phi}\tilde{\phi}}^{\text{(plat)}}|}, \quad (2.12)$$

where we evaluated $\tilde{V}_{\tilde{\phi}\tilde{\phi}}$ in the plateau region, which can be reached when $\tilde{\phi}$ climbs up the potential \tilde{V} . Here, a_{res} denotes the scale factor, when the flapping resonance takes place.

The flapping resonance generically takes place, when ω_k^2 repeatedly changes the signature. Therefore, when the scalar potential of the inflation satisfies the conditions i) and ii), the flapping resonance also takes place during reheating (see also Ref. [35]). In the early stage of reheating after small field inflation models, ω_k^2 flips the signature during each oscillation of the inflaton [36]. In this case, unlike the plateau case, the inflaton starts to oscillate around $H_{\text{osc}} \simeq m$. Then, this stage does not last long, since the inflaton exits the tachyonic region after several oscillations due to the Hubble friction [36].

2.3.3 Narrow resonance: Phase 3

In this phase, the homogeneous mode of the axion oscillates within the inflection points. During this phase, we can expand perturbatively the second derivative of the potential as

$$\tilde{V}_{\tilde{\phi}\tilde{\phi}} = 1 + \frac{1}{2}\lambda\tilde{\phi}^2 + O(\tilde{\phi}^4) \quad (2.13)$$

in a good approximation. For the α attractor type potential (2.6), λ is given by $\lambda = -4(2+3c)$. In this phase, the evolution of the homogeneous mode can be well approximated as $\tilde{\phi} = \tilde{\phi}_*(a_*/a)^{3/2} \cos \tilde{t}$, where quantities with $*$ are evaluated at the beginning of the phase 3. Using this expression, the mode equation can be rewritten as the Mathieu equation,

$$\frac{d^2 \varphi_k}{d\tilde{t}^2} + [A_k - 2q \cos 2\tilde{t}] \varphi_k = 0, \quad (2.14)$$

where we introduced

$$q \equiv -\frac{\lambda}{8} \tilde{\phi}_*^2 \left(\frac{a_*}{a}\right)^3, \quad (2.15)$$

$$A_k \equiv 1 + \left(\frac{k}{am}\right)^2 - 2q. \quad (2.16)$$

The analysis based on the Mathieu equation is possible only in the phase 3, where the homogeneous mode can be well approximated by the harmonic oscillation.

The solution of the Mathieu equation has resonance bands around $A_k \simeq n^2$ with $n = 1, 2, \dots$. In particular, the first resonance band is given by $A_k - 1 = \pm q$. This implies that for $\lambda < 0$, the resonance instability takes place for the physical wavenumbers which satisfy

$$q < \left(\frac{k}{am}\right)^2 < 3q. \quad (2.17)$$

At $a \simeq a_*$, one obtains the peak wavenumber in the first band as

$$\frac{k_{\text{peak}}}{a_* m} \simeq \sqrt{2q} \simeq \frac{\sqrt{|\lambda|} |\tilde{\phi}_*|}{2}. \quad (2.18)$$

In this phase, ω_k^2 stays all the time positive and there is no violation of the adiabatic condition, which indicates that the instability in this phase is the narrow resonance instability. The narrow resonance instability in the phase 3 proceeds much more slowly than the flapping resonance instability in the phase 2.

When the oscillation starts around $H_{\text{osc}} \simeq m$, the wavenumbers in the instability bands are red-shifted away after several oscillations. By contrast, in case $H_{\text{osc}} \ll m$, the scale factor almost does not change in one oscillation period of the zero mode and the instability modes stay in the resonance bands over many periods of oscillation. In addition, since the amplitude of $\tilde{\phi}$ and q do not decrease over many periods of the oscillation for $H_{\text{osc}}/m \ll 1$, the growth rate and the width of the resonance band do not decrease either in the time scale of the oscillation.

During the phase 2, the narrow resonance instability is not very efficient and it can be important only after entering the phase 3. This is because the oscillation period of the homogeneous mode $\tilde{\phi}$, determined by $\tilde{V}_{\tilde{\phi}\tilde{\phi}}$, still considerably changes in time during the phase 2. Since the Bose enhancement is caused by acting a regulated periodic force over many oscillation periods, the parametric resonance instability is not very efficient during the phase 2.

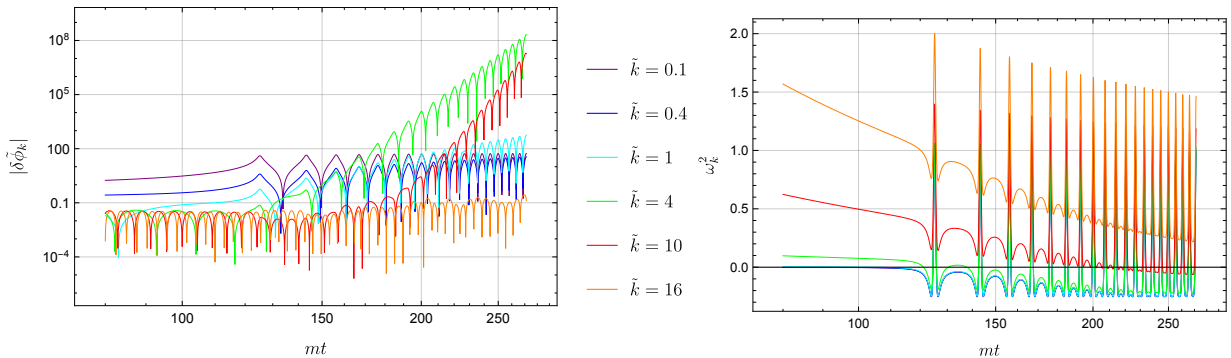


Figure 5: The left panel shows the time evolution of $\delta\tilde{\phi}_k$ for the α attractor potential with $c = 5$ and the initial condition $\tilde{\phi}_i = 3$. The right panel shows the time evolution of ω_k^2 during the same time period.

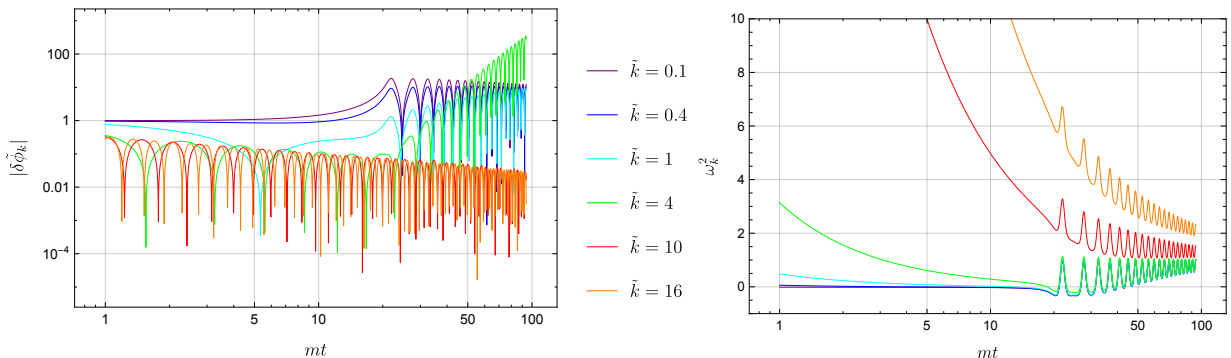


Figure 6: Same as Fig. 5 except that c is now set to $c = 0$.

2.4 Overall evolution in linear regime

In this section, we showed that the different types of instabilities become prominent during the different phases. The left panels of Fig. 5 and Fig. 6 show two typical time evolutions of $\delta\tilde{\phi}_k$ for potentials which satisfy the two conditions i) and ii). Here, again as an example, we considered the α -attractor potential with $c = 5$ (Fig. 5) and $c = 0$ (Fig. 6). In both cases, we chose the initial condition as $\tilde{\phi}_i = 3$ under the slow-roll approximation, which is the attractor solution in the plateau region. The right panels show the time evolution of ω_k^2 for each wavenumber.

When the homogeneous mode $\tilde{\phi}$ rolls down the plateau region (phase 1), ω_k^2 for the low- k modes such as $\tilde{k} = 0.1$ and $\tilde{k} = 0.4$ stay negative, leading to the tachyonic instability. Once $\tilde{\phi}$ starts to oscillate, ω_k^2 flips the signature, leading to the flapping resonance instability. The phase 2 for $c = 5$ continues longer than the one for $c = 2$ as is shown in the right panels of Fig. 5 and Fig. 6 (this can be clearly seen e.g., by looking at $\tilde{k} = 0.1$, for which $\omega_k^2 \simeq \tilde{V}_{\tilde{\phi}\tilde{\phi}}$). One of the reasons for this is because for $c = 5$ the onset of the oscillation is delayed more and the Hubble friction is less efficient. It is, however, not entirely clear

	No delay ($H_{\text{osc}}/m \simeq 1$)	Delay ($H_{\text{osc}}/m \ll 1$)
Phase 2, short	No instability	Tachyonic (\rightarrow Flapping res.) \rightarrow Narrow res.
Phase 2, long	-	Tachyonic \rightarrow Flapping res.

Table 1: This table summarizes the different instability processes for different setups. By the terms “long” and “short”, we mean the phase 2 continues over many periods of the oscillation or finishes after several oscillations.

what controls the duration of the phase 2 and this will be investigated in our future study. During the phase 3, the narrow resonance sets in. The growth rate of the narrow resonance is smaller than the flapping resonance. When the phase 2 continues sufficiently long, the energy transfer from the homogeneous mode to the inhomogeneous mode finishes before entering the phase 3. Therefore, depending on how long the phase 2 persists, the dominant instability and the resultant spectrum will be different (see Table 1).

3. Lattice simulation

In the previous section, we discussed the evolution of the inhomogeneous mode based on linear analysis. When we neglect the non-linear contributions, the energy transfer from the homogeneous mode to the inhomogeneous modes eternally continues, which is obviously wrong. In fact, once the inhomogeneous modes become comparable to the homogeneous mode, the backreaction and the rescattering turn on and the dynamics enters a highly non-linear regime. In this section, we address the non-linear dynamics based on the lattice simulation.

3.1 Nonlinear dynamics of the axion

Here we solve the field equation (2.4) directly in the lattice space where the spatial derivative is replaced with the finite difference. For computational convenience, we use the conformal time, τ as a time variable, defined by $d\tau = dt/a$ instead of the cosmic time and in order to remove the Hubble friction term, we redefine the field variable as $\tilde{\phi} = \tilde{\Phi}/a$. Then, the equation of motion (2.4) can be rewritten as

$$\tilde{\Phi}'' - \partial_{\mathbf{x}}^2 \tilde{\Phi} - \frac{a''}{a} \tilde{\Phi} + a^3 \tilde{V}_{\tilde{\phi}} = 0, \quad (3.1)$$

where the prime ($\tilde{\Phi}'$) expresses the derivative with respect to the normalized conformal time $m\tau$. We have solved the above equation by using fourth order Symplectic integrator with 256^3 grids for the α attractor type potential in the radiation dominated Universe, $a \propto \tau$. We start to solve the lattice simulation at the time when $H = m$, again setting $a_{H=m} = 1$, i.e. $m\tau_i = 1$, and imposing the slow-roll condition¹. The simulation box size is set to $2\pi m^{-1}$.

Fig. 7 and 8 show the evolution of the homogeneous mode, i.e. spatially-averaged field value (red), the root-mean-squared of the field fluctuation (green), the energy density

¹As was discussed in the previous section, this can be verified in the case of our interest where the axion was initially located at the plateau region.

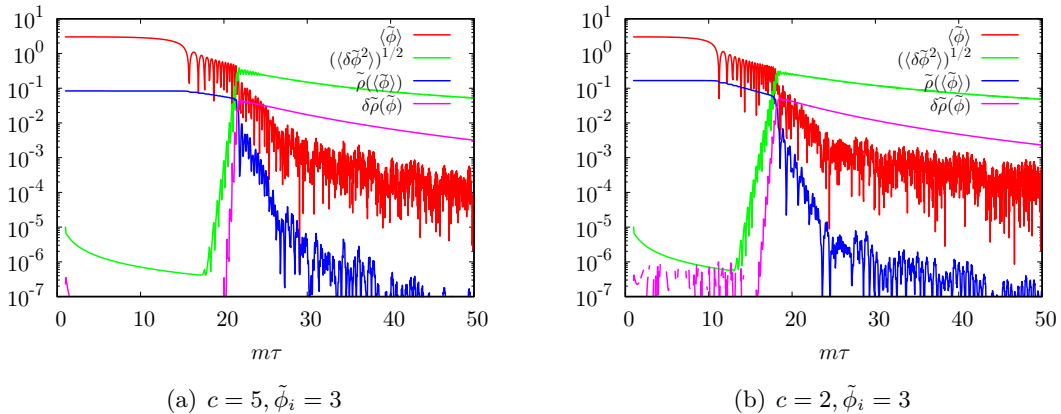


Figure 7: Evolution of the spatial average of $\tilde{\phi}$ (red), the root-mean-square $\langle \delta\tilde{\phi}^2 \rangle^{1/2}$ (green), the energy density of the average $\tilde{\rho}(\langle \tilde{\phi} \rangle)$ (blue), energy density perturbation, $\langle \delta\tilde{\rho}^2 \rangle^{1/2}$ (orange). We have taken $c = 5$ ($c = 2$) and $\tilde{\phi}_i = 3$ in the left (right) panel.

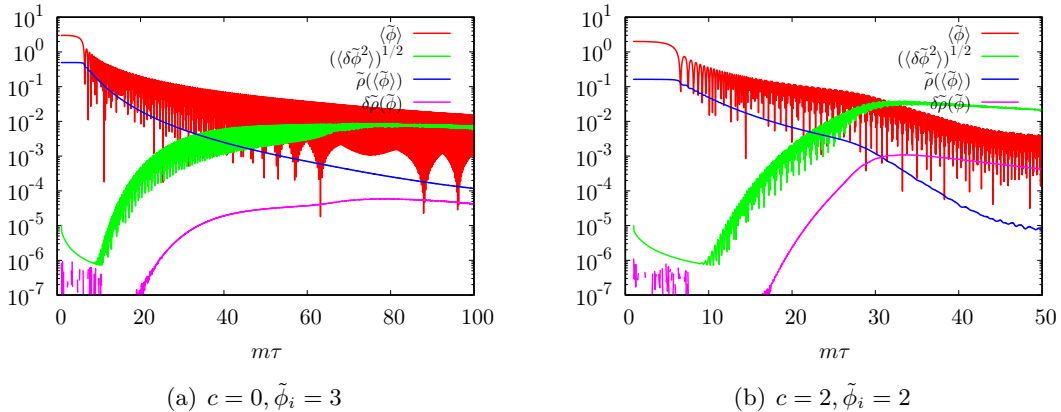


Figure 8: Same as Fig. 7 but $c = 0$ and $\tilde{\phi}_i = 3$ in the left panel and $c = 2$ and $\tilde{\phi}_i = 2$ in the right panel.

of the homogeneous mode (blue) and the energy density fluctuation (magenta). After the (delayed) onset of the axion oscillation, the field fluctuation grows exponentially and it eventually dominates over the homogeneous component (except for the case with $c = 0$ and $\tilde{\phi}_i = 3$). At that time, the exponential growth stops due to the backreaction from produced inhomogeneous modes on the homogeneous mode. Fig. 7 shows that, through the flapping resonance in phase 2, the fluctuation grows quickly and saturates in a short time period. On the other hand, Fig. 8 shows the growth due to the narrow resonance regime in phase 3. In this case, the growth rate is smaller than that of the flapping resonance and it takes longer time for fluctuations to catch up with the zero mode or fluctuations never catch up with the zero mode as can be seen in Fig. 8(a)

To see the spectrum of the enhanced nonzero k -mode axion, let us consider the Fourier

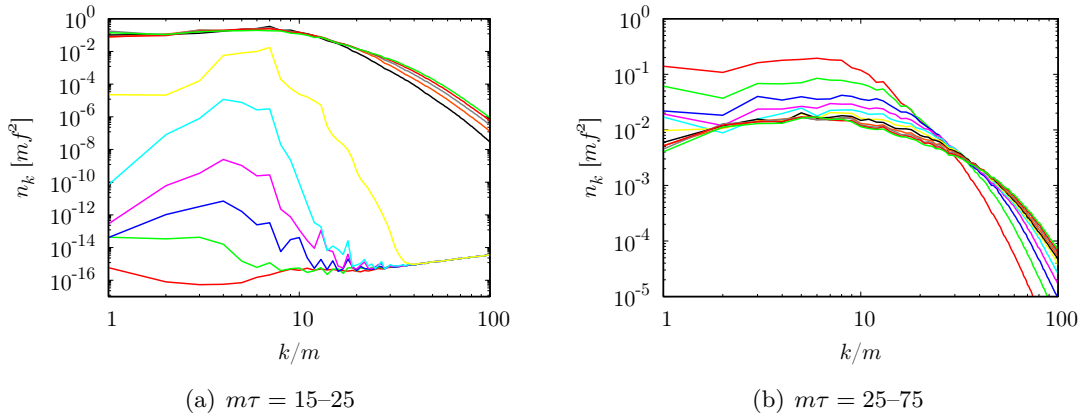


Figure 9: Evolution of the occupation number of the axion for $m\tau = 15-25$ (left), $25-75$ (right) in terms of the conformal time. Time evolves from bottom (top) to top (bottom) in the left (right) panel. We have taken $c = 5$ and $\tilde{\phi}_i = 3$.

transformation, $\Phi_{\mathbf{k}}$, and define the occupation number (normalized by mf^2) as

$$n_k = \frac{1}{2} \left(\frac{|\tilde{\Phi}'_{\mathbf{k}}|^2}{\Omega_k} + \Omega_k |\tilde{\Phi}_{\mathbf{k}}|^2 \right), \quad (3.2)$$

where Ω_k is defined by²

$$\Omega_k^2 = \left(\frac{k}{m} \right)^2 + a^2 \langle \tilde{V}_{\tilde{\phi}\tilde{\phi}} \rangle. \quad (3.3)$$

Fig. 9, 10, and 11 show the spectrum of n_k . Different curves represent spectra at different time steps. In Fig. 9 and 10, the peak modes grow through the flapping resonance and in Fig. 11, the peak mode grows through the narrow resonance. When the energy density in inhomogeneous modes roughly catches up with the one in the homogeneous mode, the growth of the inhomogeneous modes terminates and the peaked spectrum starts to be redistributed by rescattering. As discussed in the context of reheating, e.g., by Micha and Tkachev [37,38], the turbulence drives the momentum flow to larger wavenumbers. The flow to UV modes is also found in our lattice simulation.

3.2 Oscillon formation

The plateau condition, the condition ii), which is crucial for a delayed onset of the oscillation and succeeding instabilities, requires that the absolute value of the potential gradient, $|\tilde{V}'_{\tilde{\phi}}|$, should be smaller than the one for the quadratic potential, given by $|\tilde{\phi}|$, i.e., the potential \tilde{V} should be shallower than the one for the quadratic one. This condition agrees with the often-said condition for the oscillon formation from various case studies [31,39]. Indeed, we found from our lattice simulation that, once the contribution from nonzero modes of the axion field becomes sufficiently larger than that from the homogeneous mode, the axion

²In order to avoid imaginary numbers in our numerical computation, we set $\langle \tilde{V}_{\tilde{\phi}\tilde{\phi}} \rangle = 1$, which corresponds to the value when the homogeneous mode of the axion is around the potential minimum during each oscillation.

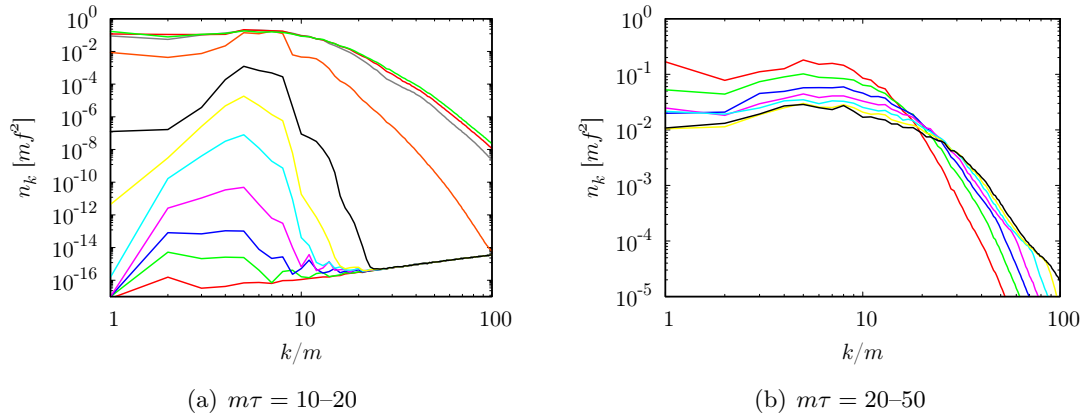


Figure 10: Evolution of the occupation number of the axion for $m\tau = 10-20$ (left), $20-50$ (right). Time evolves from bottom (top) to top (bottom) in the left (right) panel. We have taken $c = 2$ and $\tilde{\phi}_i = 3$.

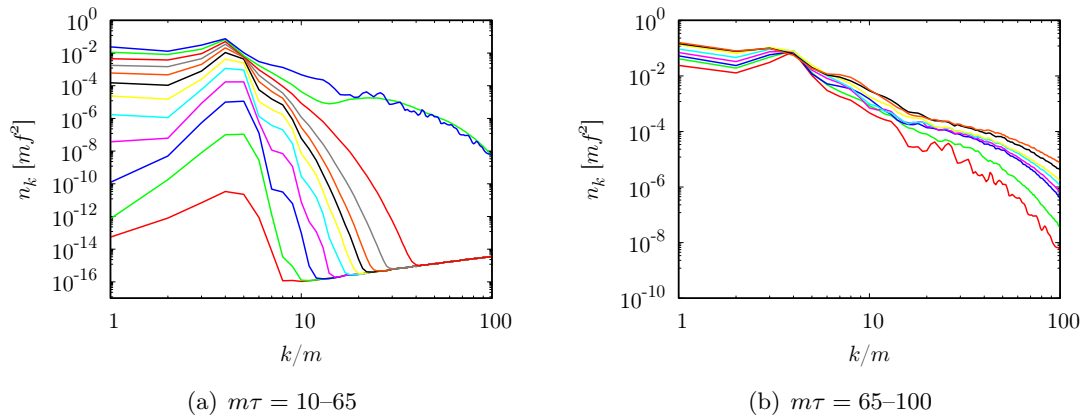


Figure 11: Evolution of the occupation number of the axion for $m\tau = 10-65$ (left), $65-100$ (right). Time evolves from bottom (top) to top (bottom) in the both panels. We have taken $c = 0$ and $\tilde{\phi}_i = 3$.

field forms oscillons, which are almost spherically symmetric. Fig. 12 shows snapshots of energy density fluctuation of the axion. It shows that the oscillon formation occurs around $m\tau \sim 40$. Note that the energy of the axion is mostly stored in oscillons after copious oscillons are formed.

4. GW emission

In this section, we consider GW emission sourced by axion field fluctuations. In general, a scalar perturbation does not source GWs in the linear perturbation theory (at a perturbed FRW spacetime), but it is not the case in the non-linear regime. When the axion was initially located at a plateau region, the instabilities discussed in the previous sections can lead to a prominent emission of GWs.

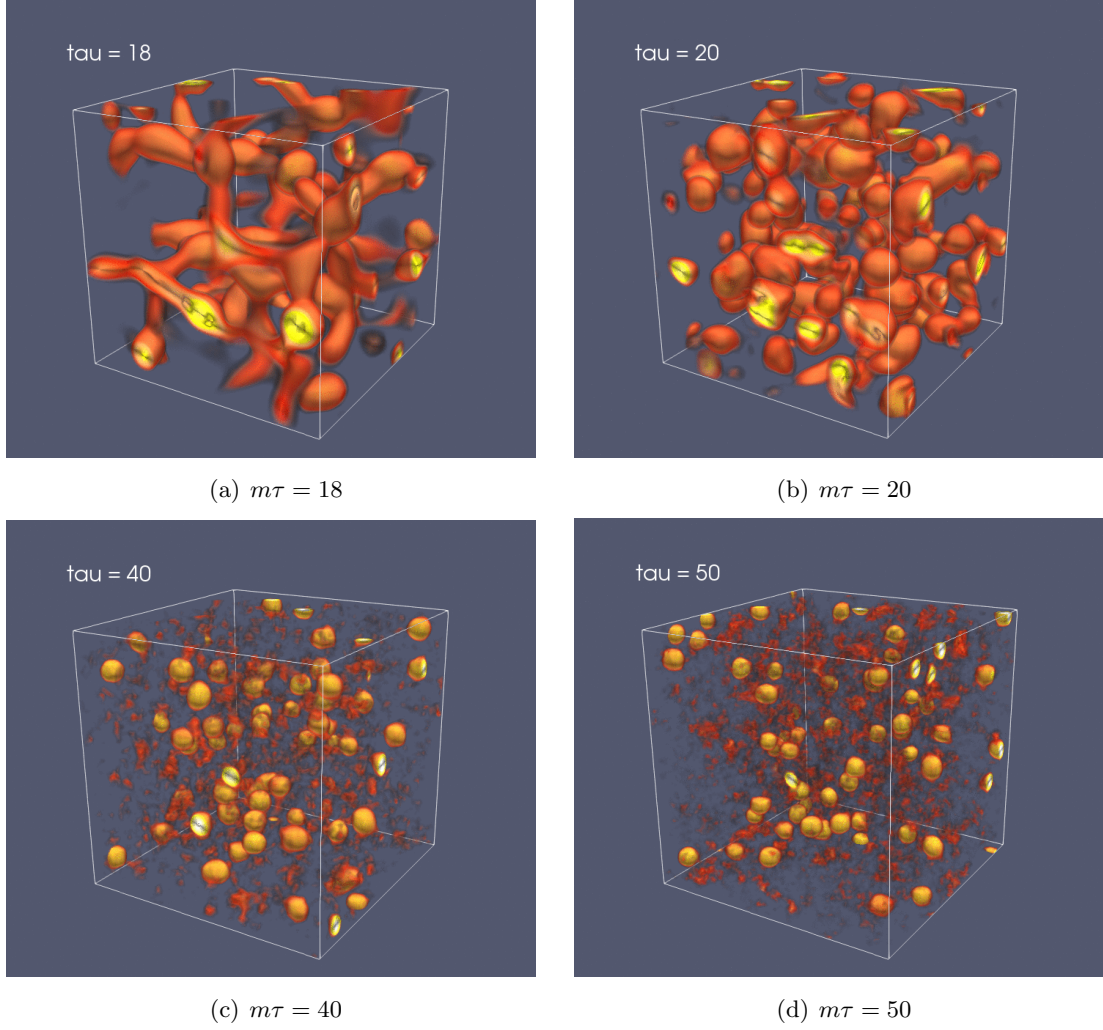


Figure 12: Snapshots of the evolution of the axion energy density in 3-dimensional lattice space for $m\tau = 18$ (upper left), 20 (upper right), 40 (lower left), and 50 (lower right). The red, yellow and white region correspond to $\rho/\bar{\rho} > 2, 4$ and 10 respectively with $\bar{\rho}$ being the spatial average of the axion energy density. We have taken $c = 5$ and $\tilde{\phi}_i = 2$.

4.1 GW spectrum

To compute the stochastic background of GWs, we consider the line element with the tensor metric perturbations, h_{ij} :

$$ds^2 = -dt^2 + a^2(\delta_{ij} + h_{ij})dx^i dx^j, \quad (4.1)$$

where we neglect the scalar and vector metric perturbations. Note that h_{ij} satisfies the transverse-traceless condition, $\partial_i h_{ij} = 0$ and $h_{ii} = 0$. The linearized Einstein equation gives the evolution of the tensor metric perturbation,

$$\ddot{h}_{ij} + 3H\dot{h}_{ij} - \frac{1}{a^2}\nabla^2 h_{ij} = \frac{2}{M_{\text{P}}^2}\Pi_{ij}^{\text{TT}}, \quad (4.2)$$

where Π_{ij}^{TT} is the anisotropic stress tensor with the transverse-traceless (TT) projection. Using the tensor perturbation h_{ij} , one can obtain the energy density of the stochastic GW background as follows,

$$\rho_{\text{GW}}(t) = \frac{M_{\text{P}}^2}{4} \langle \dot{h}_{ij} \dot{h}_{ij} \rangle. \quad (4.3)$$

Let us redefine the tensor mode as $h_{ij} = \bar{h}_{ij}/a$ and rewrite Eq.(4.2) in terms of the conformal time,

$$\bar{h}_{ij}'' - \partial_{\mathbf{x}}^2 \bar{h}_{ij} - \frac{a''}{a} \bar{h}_{ij} = 2a^3 \left(\frac{f}{M_{\text{P}}} \right)^2 \tilde{\Pi}_{ij}^{\text{TT}}, \quad (4.4)$$

with $\tilde{\Pi}_{ij}^{\text{TT}} = \Pi_{ij}^{\text{TT}}/(mf)^2$.

In our lattice calculation, instead of directly solving Eq.(4.4), we solve the following evolution equation of u_{ij} ,

$$u_{ij}'' - \partial_{\mathbf{x}}^2 u_{ij} - \frac{a''}{a} u_{ij} = 2a^3 \left(\frac{f}{M_{\text{P}}} \right)^2 \tilde{\Pi}_{ij}, \quad (4.5)$$

where $\tilde{\Pi}_{ij}$ is the source term before applying the TT projection which is given by $\tilde{\Pi}_{ij} = \partial_i \tilde{\phi} \partial_j \tilde{\phi}$. One can obtain \bar{h}_{ij} by operating the TT projection on u_{ij} in the Fourier space after solving Eq.(4.5). In this way, we obtain the same solution as the one obtained by directly solving Eq.(4.4) [17].

The TT projection can be simply defined in the Fourier space, in which the TT projection operator is given by

$$\Lambda_{ijklm}(\hat{\mathbf{k}}) = P_{il}(\hat{\mathbf{k}})P_{jm}(\hat{\mathbf{k}}) - \frac{1}{2}P_{ij}(\hat{\mathbf{k}})P_{lm}(\hat{\mathbf{k}}), \quad (4.6)$$

with $P_{ij}(\hat{\mathbf{k}}) = \delta_{ij} - \hat{k}_i \hat{k}_j$ and $\hat{\mathbf{k}} = \mathbf{k}/|\mathbf{k}|$. Using the projection operator, we obtain the Fourier mode of the tensor perturbation as

$$h_{ij}(\mathbf{k}) = \frac{1}{a} \Lambda_{ijklm}(\hat{\mathbf{k}}) u_{lm}(\mathbf{k}). \quad (4.7)$$

The energy density of the stochastic GW background can be rewritten in terms of the Fourier transform,

$$\rho_{\text{GW}} = \frac{M_{\text{P}}^2}{4L^3} \int d^3k \dot{h}_{ij}(\mathbf{k}) \dot{h}_{ij}^*(\mathbf{k}), \quad (4.8)$$

where L is the size of the Universe. Finally, the spectrum of GW density parameter in terms of the frequency, ν , can be calculated as

$$\Omega_{\text{GW}}(\nu) = \frac{1}{\rho_c} \frac{d\rho_{\text{GW}}}{d \ln \nu}, \quad (4.9)$$

where ρ_c denotes the total energy density, given by $\rho_c = 3H^2 M_{\text{P}}^2$.

We solved Eq.(4.5) together with Eq.(3.1) in 3-dimensional lattice space with the same setup in the previous section and calculated the spectrum using the above formula. Fig. 13 and 14 show the evolution of the spectrum of GW density parameter. They show that for $(c, \tilde{\phi}_i) = (5, 3)$ and $(2, 3)$, the peak wavenumber is around $k_{\text{peak}} \simeq 10m$, which is roughly

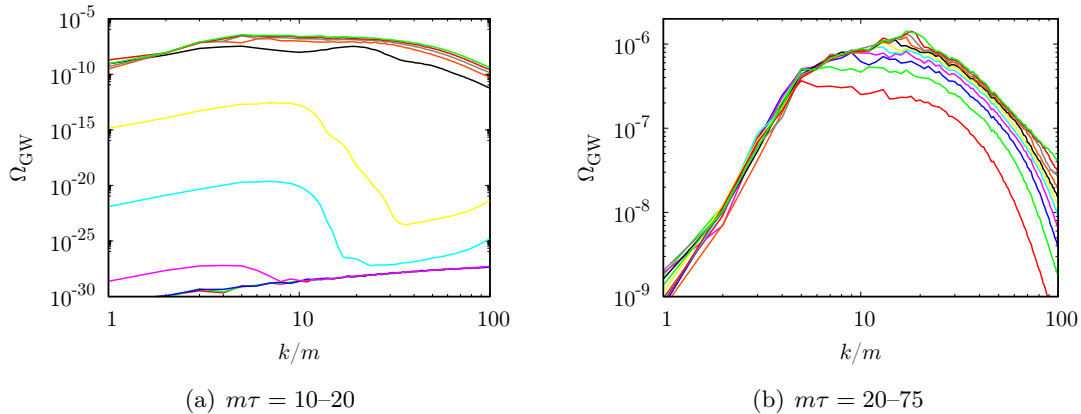


Figure 13: Evolution of the power spectrum of the density parameter of GW. Time evolves from bottom to top in both panels. We have taken $f = 10^{16}$ GeV, $c = 5$ and $\tilde{\phi}_i = 3$.

twice as large as the peak wave number of the spectrum of n_k before the rescattering. We found that the GW emission stops around $m\tau \sim 40$, which corresponds to the time of oscillon formation as shown in the previous section. Because the axion field configuration becomes almost spherically symmetric after the oscillon formation, GWs are no longer emitted after that [40].

The GWs emitted from a scalar field which was located at a plateau region has been sometimes described as “the GWs from oscillons” [41–43]. However, this is somehow misleading, because the prominent GW emission takes place prior to the formation of the oscillons. In fact, the efficient GW emission stops after the oscillons formed and the spectrum of the GWs gets decoupled from the spectrum of the axion number density, where the momentum transfer still continues. (Related to this, see a recent publication [44].)

4.2 GW forest

So far, we have computed the spectra of the axion and GWs without specifying the axion mass because the evolution equations do not depend explicitly on the axion mass if we use dimensionless time and spatial coordinates normalized by the axion mass. However, the onset time of the axion oscillation is determined by the axion mass and thus the current frequency of the emitted GWs depends on the axion mass. For our convenience, let us introduce κ , using the peak physical frequency ω_{phys} as

$$\kappa \equiv \frac{\omega_{\text{phys}}}{m} = \frac{k_{\text{peak}}^{\text{em}}}{m a_{\text{em}}}. \quad (4.10)$$

As discussed in the previous section, after the rescattering becomes important, the turbulence drives the momentum flow to UV. Taking into account those, we can express κ as

$$\kappa = \frac{k_{\text{peak}}^{\text{res}}}{m a_{\text{res}}} \times \frac{k_{\text{peak}}^{\text{em}}/a_{\text{em}}}{k_{\text{peak}}^{\text{res}}/a_{\text{res}}}. \quad (4.11)$$

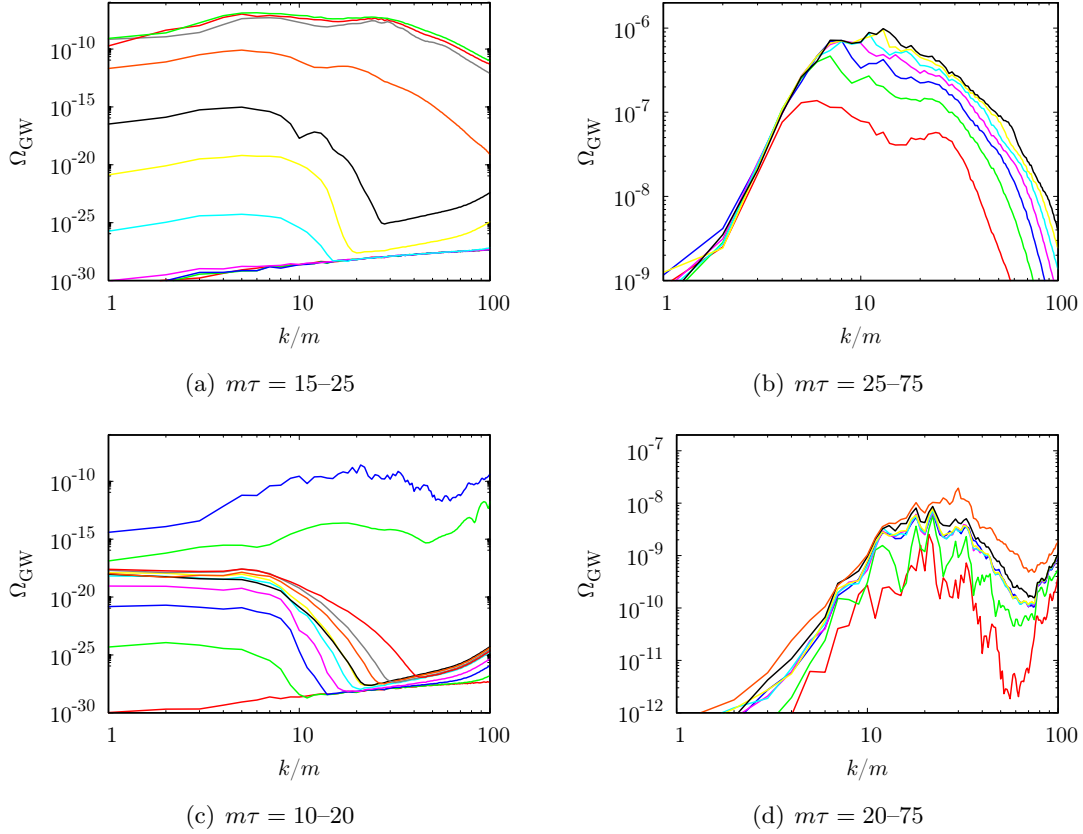


Figure 14: Same as Fig. 13 but $c = 2$ (top panels) and $c = 0$ (bottom panels).

When the dominant instability process is the flapping resonance, $k_{\text{peak}}^{\text{res}}/(m a_{\text{res}})$ is given by Eq. (2.12) and when it is the narrow resonance, $k_{\text{peak}}^{\text{res}}/(m a_{\text{res}})$ is given by Eq. (2.18). The second factor $(k_{\text{peak}}^{\text{em}}/a_{\text{em}})/(k_{\text{peak}}^{\text{res}}/a_{\text{res}})$ describes the momentum flow due to the turbulence.

Using κ , the redshifted frequency of GWs today is given by

$$\nu_0 = \frac{\kappa m}{2\pi} \left(\frac{a_{\text{em}}}{a_0} \right). \quad (4.12)$$

When an axion emitted GWs during radiation domination, we obtain

$$\nu_0 = \frac{\kappa m}{2\pi} \times \left(\frac{\rho_{r,0}}{\rho_{r,\text{em}}} \right)^{1/4} \simeq 0.78 \text{ nHz } \kappa \left(\frac{m}{H_{\text{em}}} \right)^{1/2} \left(\frac{m}{10^{-12} \text{ eV}} \right)^{1/2}, \quad (4.13)$$

where we approximated $\rho_{r,\text{em}}$ as $\rho_{r,\text{em}} \simeq \rho_{\text{em}}$ and used $H_0 = 100 h \text{ km s}^{-1} \text{ Mpc}^{-1} = 2.13 h \times 10^{-33} \text{ eV}$, $\Omega_r h^2 \simeq 2.47 \times 10^{-5}$, and $1 \text{ Hz} = 6.58 \times 10^{-16} \text{ eV}$. Similarly, when an axion emitted GWs during (late time) matter domination, we obtain

$$\nu_0 = \frac{\kappa m}{2\pi} \times \left(\frac{\rho_{m,0}}{\rho_{m,\text{em}}} \right)^{1/3} \simeq 2.1 \times 10^{-18} \text{ Hz } \kappa \left(\frac{m}{H_{\text{em}}} \right)^{2/3} \left(\frac{m}{10^{-30} \text{ eV}} \right)^{1/3} \quad (4.14)$$

where we approximated $\rho_{m,\text{em}}$ as $\rho_{m,\text{em}} \simeq \rho_{\text{em}}$ and used $\Omega_m h^2 \simeq 0.14$ [45].

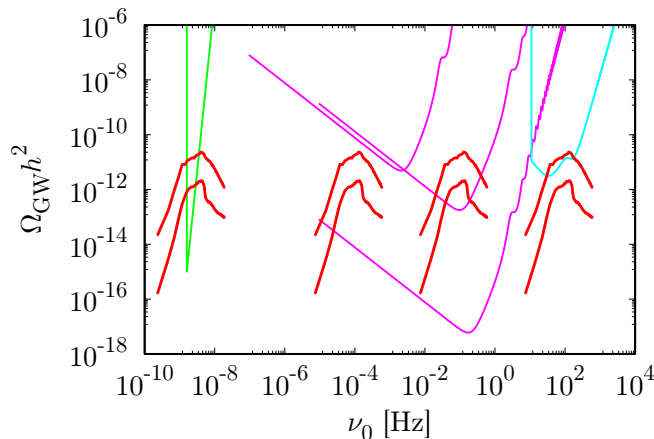


Figure 15: Predicted density spectrum of GWs (thick red lines) and sensitivity curves of SKA, LISA, DECIGO (ultimate-DECIGO) and ET from left to right. We have taken $f = 10^{16}$ GeV, $c = 5$ and the axion mass is set to be $m = 10^{-15}$ eV, 10^{-6} eV, 1 eV and 10^6 eV from left to right and $\phi_i = 3$ and 2 from top to bottom.

String theory predicts axions in various mass scales. When these axions were located at a plateau region before they start to oscillate, our discussion here predicts GW emissions with various frequencies, dubbed *Gravitational wave forest*. Figure 15 shows the density spectrum of GWs from axions with different mass scales and their detectability by current and future multi-band GW detectors [4, 5]. In Fig. 15, we chose the decay constant f as $f = 10^{16}$ GeV as is typically the case for stringy axions [7]. When we change f , Ω_{GW} scales as $\Omega_{\text{GW}} \propto f^4$.

4.3 GWs from axion dark matter

In the previous subsection, we discussed the spectrum of GWs emitted from axions for a fixed value of f . In case axions do not decay into other species and they are just adiabatically diluted after the emission of GWs, their abundances should be compatible with the thermal history of the Universe later on [46].

For our illustrative purpose, here let us consider the case when the potential of the axion after the onset of the oscillation can be approximated by a power-law form as $\tilde{V}(\tilde{\phi}) \propto \tilde{\phi}^n$. Using this potential, here, we discuss a crude evaluation of Ω_{GW} based on an order estimation to understand which quantity is important for enhancing Ω_{GW} . A prominent emission of GWs takes place, roughly when the energy is distributed equally between the homogeneous mode and the inhomogeneous mode, i.e.,

$$\left| \frac{\delta\rho_{\text{em}}}{\rho_{\text{em}}(\langle\phi\rangle)} \right| \simeq \mathcal{O}(1), \quad (4.15)$$

which roughly implies $|\delta\phi| \simeq |\langle\phi\rangle|$. Then, using³ $|\langle\phi_{\text{em}}\rangle| \simeq f(a_{\text{osc}}/a_{\text{em}})^{6n/(n+2)}$, we obtain

³For $\tilde{V} \propto \tilde{\phi}^n$, the equation of state for the homogeneous mode of the axion is given by $\omega = (n-2)/(n+2)$. Then, the homogeneous modes of $\tilde{\phi}$ and the energy density $\tilde{\rho}$ scale as $\tilde{\phi} \propto a^{-6/(n+2)}$ and $\tilde{\rho} \propto a^{-6n/(n+2)}$.

the amplitude of the GWs emitted at $a \simeq a_{\text{em}}$ as (we drop the tensor indices),

$$|h_{\text{em}}| \simeq 2\Delta \left(\frac{f}{M_P} \right)^2 \left(\frac{a_{\text{osc}}}{a_{\text{em}}} \right)^{12/(n+2)}, \quad (4.16)$$

where Δ quantifies the efficiency of the GW emission from the inhomogeneous mode of the axion and takes a value in the range $0 \leq \Delta < 1$. In particular, for a GW emission after formations of oscillons, which are almost spherically symmetric, $|h_{\text{em}}|$ is highly suppressed by $\Delta \ll 1$.

Using Eq. (4.16), the energy density of GWs at the peak wavenumber is given by

$$\rho_{\text{GW,em}} \simeq \frac{M_P^2 \omega_{\text{phys}}^2}{4} (h_{\text{em}})^2 \simeq \Delta^2 (\kappa m)^2 \frac{f^4}{M_{\text{pl}}^2} \left(\frac{a_{\text{osc}}}{a_{\text{em}}} \right)^{24/(n+2)}. \quad (4.17)$$

Dividing this expression by the energy density of radiation at $a = a_{\text{em}}$, we obtain

$$\frac{\rho_{\text{GW},0}}{\rho_{r,0}} \simeq \frac{\rho_{\text{GW,em}}}{\rho_{r,\text{em}}} \simeq \frac{\kappa^4 \Delta^2}{M_P^2} \frac{1}{(2\pi\nu_0)^2} \frac{(\rho_{\text{em}})^2}{\rho_{r,\text{em}}} \left(\frac{a_{\text{em}}}{a_0} \right)^2 \left(\frac{a_{\text{osc}}}{a_{\text{em}}} \right)^{\frac{12(2-n)}{2+n}}, \quad (4.18)$$

where we used $\rho_{\text{em}} \simeq \rho_{\text{osc}} (a_{\text{osc}}/a_{\text{em}})^{6n/(n+2)}$. In particular when the phase 2 continues long, we cannot express the potential in terms of a single power law term $\tilde{\phi}^n$. However, Eq. (4.18) is somewhat instructive. For $|\tilde{\phi}| \gtrsim 1$, the potential \tilde{V} is shallower than $\tilde{\phi}^2$. Equation (4.18) tells us that the emitted GWs are more suppressed for $n < 2$, when it takes longer until the emission of the GWs after the onset of the oscillation. This suppression can be evaded, either in case $a_{\text{osc}} \simeq a_{\text{em}}$ or (even if $a_{\text{em}} \gg a_{\text{osc}}$) in case the phase 2 finishes soon and the dominant instability process takes place during the phase 3.

For a simplistic estimation, here let us consider the case when we can approximate the potential as $\tilde{V} \simeq \tilde{\phi}^2/2$ soon after $\tilde{\phi}$ starts to oscillate. (We end up with the same estimation, when $a_{\text{osc}} \simeq a_{\text{em}}$ and \tilde{V} can be approximated as the quadratic one after the GW emission.) Then, multiplying $\Omega_r h^2$ on Eq. (4.18) with $n = 2$, we obtain

$$\Omega_{\text{GW}} h^2 \simeq \frac{3\kappa^4 \Delta^2}{(2\pi\nu_0)^2} \left(\frac{H_0}{h} \right)^2 (\Omega_\phi h^2)^2 \simeq 0.8 \times 10^{-18} \kappa^4 \Delta^2 \left(\frac{\text{nHz}}{\nu_0} \right)^2 (\Omega_\phi h^2)^2. \quad (4.19)$$

Since $\Delta < 1$ and $\Omega_\phi h^2 \leq \Omega_{\text{CDM}} h^2 \simeq 0.12$, this estimation reads

$$\Omega_{\text{GW}} h^2 < 1.6 \times 10^{-16} \left(\frac{\kappa}{10} \right)^4 \left(\frac{\text{nHz}}{\nu_0} \right)^2, \quad (4.20)$$

indicating that to reach $\Omega_{\text{GW}} h^2 \sim 10^{-16}$ at $\nu_0 = \text{nHz}$, κ should be larger than 10. At lower frequencies than nHz, Ω_{GW} is enhanced as $\propto 1/\nu_0^2$. To detect GWs in this frequency range, we will need a new window of GW detections which fills the gap between CMB and PTA observations [6]. Figure 16 shows $\Omega_{\text{GW}} h^2$ computed from the lattice simulation for the α attractor potential with $c = 5$ and $\tilde{\phi}_i = 2, 3$, when $\Omega_\phi = \Omega_{\text{CDM}}$ and $n = 2$.

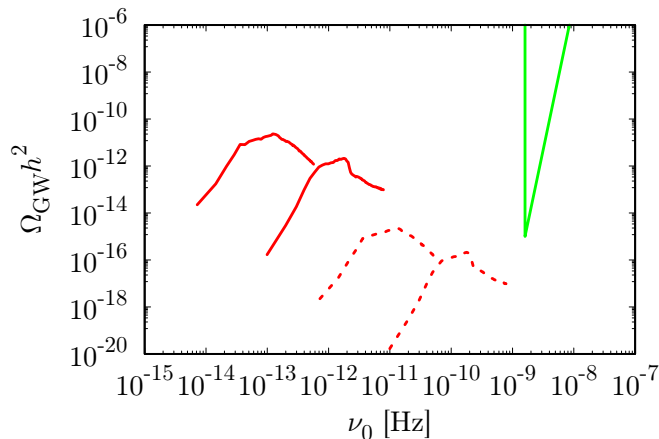


Figure 16: Same as Fig. 15 but the present abundance of the axion is fixed to be the dark matter abundance. The dashed lines correspond to $f = 10^{15}$ GeV.

5. Conclusion

In this paper, we analyzed the dynamics of string axions which were initially located at a plateau region in their scalar potentials. After the delayed onset of the axion oscillation, different instabilities take place, depending on different phases which are characterized by the signature of $\tilde{V}_{\phi\tilde{\phi}}$. In particular, when the tachyonic instability repeatedly turns on and off, the field fluctuation is resonantly enhanced (flapping resonance). The flapping resonance can more efficiently amplify the field fluctuation than the narrow resonance. In addition, when the plateau condition, the condition ii), is fulfilled, oscillons are rather generically formed as a consequence of resonant instabilities. This was also verified in our lattice simulation. Such a resonant amplification of the axion fluctuation can lead to a copious emission of GWs, providing a new source of gravitational wave background. The GW emission lasts also after the saturation of the exponential growth but terminates after the oscillon formation.

In the context of string axiverse, there are plenty of axions whose mass spectrum spreads over many orders of magnitude. When some of the axions were located at plateau regions before they start to oscillate, significant amounts of GWs can be emitted in various frequency bands, corresponding to their mass scales (*GW forest*). Axions with $f \sim 10^{16}$ GeV, which are typically predicted in string theory, lead to detectable GWs. This can open up a new window to probe string axiverse by means of future multi-band GW observations.

One caveat is that string axions with $f \sim 10^{16}$ GeV overclose the Universe, when they are long-lived. This problem can be circumvented, if these axions decay, e.g., due to an enhanced coupling with gauge fields. It occurs e.g. in clockwork/aligned axion model [47] and the model with gauge kinetic mixing [48]. In addition, a moderately large coupling to (hidden) gauge fields can suppress the final axion abundance through efficient dissipation of the axion energy into gauge field [49,50]. It potentially opens the possibility to generate

GWs in the reach of pulsar timing observation.

A sizable coupling between axions and gauge fields can alter the GW emission process. In this case, the axion can produce gauge fields explosively and the backreaction from the produced gauge fields yields efficient production of the nonzero mode axions [50]. In that case, both axion and gauge field can source GWs [51]. In particular, GW emission continues even after the oscillon formation because of the efficient gauge field production inside the oscillon and it predicts GWs with higher frequency range. We will report this result in our future study [52].

Acknowledgments

We would like to thank K. Kamada and M. Yamazaki for helpful discussions. N. K. acknowledges the support by Grant-in-Aid for JSPS Fellows. J. S. was in part supported by JSPS KAKENHI Grant Numbers JP17H02894, JP17K18778, JP15H05895, JP17H06359, JP18H04589. J. S and Y. U. are also supported by JSPS Bilateral Joint Research Projects (JSPS-NRF collaboration) String Axion Cosmology. Y. U. is supported by JSPS Grant-in-Aid for Research Activity Start-up under Contract No. 26887018, Grant-in-Aid for Scientific Research on Innovative Areas under Contract Nos. 16H01095 and 18H04349, and Grant-in-Aid for Young Scientists (B) under Contract No. 16K17689. Y. U. is also supported in part by Building of Consortia for the Development of Human Resources in Science and Technology and Daiko Foundation.

References

- [1] B. P. Abbott *et al.* [LIGO Scientific and Virgo Collaborations], *Phys. Rev. Lett.* **116**, no. 6, 061102 (2016) doi:10.1103/PhysRevLett.116.061102 [arXiv:1602.03837 [gr-qc]].
- [2] P. A. R. Ade *et al.* [POLARBEAR Collaboration], *Astrophys. J.* **848**, no. 2, 121 (2017) doi:10.3847/1538-4357/aa8e9f [arXiv:1705.02907 [astro-ph.CO]].
- [3] T. Matsumura *et al.*, *J. Low. Temp. Phys.* **176**, 733 (2014) doi:10.1007/s10909-013-0996-1 [arXiv:1311.2847 [astro-ph.IM]].
- [4] P. Amaro-Seoane *et al.*, *GW Notes* **6**, 4 (2013). N. Seto, S. Kawamura and T. Nakamura, *Phys. Rev. Lett.* **87**, 221103 (2001)
- [5] J. Aasi *et al.* [LIGO Scientific Collaboration], *Class. Quant. Grav.* **32**, 074001 (2015). F. Acernese *et al.* [VIRGO Collaboration], *Class. Quant. Grav.* **32**, no. 2, 024001 (2015). K. Somiya [KAGRA Collaboration], *Class. Quant. Grav.* **29**, 124007 (2012)
- [6] S. L. Detweiler, “Pulsar timing measurements and the search for gravitational waves,” *Astrophys. J.* **234**, 1100 (1979). L. Lentati *et al.*, “European Pulsar Timing Array Limits On An Isotropic Stochastic Gravitational-Wave Background,” *Mon. Not. Roy. Astron. Soc.* **453**, no. 3, 2576 (2015). [arXiv:1504.03692 [astro-ph.CO]]. Z. Arzoumanian *et al.* [NANOGrav Collaboration], “The NANOGrav Nine-year Data Set: Limits on the Isotropic Stochastic Gravitational Wave Background,” *Astrophys. J.* **821**, no. 1, 13 (2016). [arXiv:1508.03024 [astro-ph.GA]].
- [7] P. Svrcek and E. Witten, *JHEP* **0606**, 051 (2006) doi:10.1088/1126-6708/2006/06/051 [hep-th/0605206].

- [8] J. P. Conlon, F. Quevedo and K. Suruliz, JHEP **0508**, 007 (2005). J. Halverson, C. Long and P. Nath, arXiv:1703.07779 [hep-ph].
- [9] A. Arvanitaki, S. Dimopoulos, S. Dubovsky, N. Kaloper and J. March-Russell, Phys. Rev. D **81**, 123530 (2010).
- [10] J. Soda and Y. Urakawa, arXiv:1710.00305 [astro-ph.CO].
- [11] S. Dubovsky, A. Lawrence and M. M. Roberts, JHEP **1202**, 053 (2012)
- [12] Y. Nomura, T. Watari and M. Yamazaki, arXiv:1706.08522 [hep-ph].
- [13] L. Kofman, A. D. Linde and A. A. Starobinsky, Phys. Rev. Lett. **73**, 3195 (1994) doi:10.1103/PhysRevLett.73.3195 [hep-th/9405187].
- [14] L. Kofman, A. D. Linde and A. A. Starobinsky, Phys. Rev. D **56**, 3258 (1997) doi:10.1103/PhysRevD.56.3258 [hep-ph/9704452].
- [15] S. Y. Khlebnikov and I. I. Tkachev, Phys. Rev. D **56**, 653 (1997) doi:10.1103/PhysRevD.56.653 [hep-ph/9701423].
- [16] D. G. Figueroa and F. Torrenti, JCAP **1710**, no. 10, 057 (2017) doi:10.1088/1475-7516/2017/10/057 [arXiv:1707.04533 [astro-ph.CO]].
- [17] J. Garcia-Bellido, D. G. Figueroa and A. Sastre, Phys. Rev. D **77**, 043517 (2008) doi:10.1103/PhysRevD.77.043517 [arXiv:0707.0839 [hep-ph]].
- [18] E. Witten, Nucl. Phys. B **156**, 269 (1979).
- [19] E. Witten, Annals Phys. **128**, 363 (1980).
- [20] K. Yonekura, JCAP **1410**, no. 10, 054 (2014) doi:10.1088/1475-7516/2014/10/054 [arXiv:1405.0734 [hep-th]].
- [21] Y. Nomura and M. Yamazaki, Phys. Lett. B **780**, 106 (2018) doi:10.1016/j.physletb.2018.02.071 [arXiv:1711.10490 [hep-ph]].
- [22] P. A. R. Ade *et al.* [Planck Collaboration], Astron. Astrophys. **594**, A20 (2016) doi:10.1051/0004-6361/201525898 [arXiv:1502.02114 [astro-ph.CO]].
- [23] G. Shiu and W. Staessens, arXiv:1807.00620 [hep-th].
- [24] G. Shiu and W. Staessens, arXiv:1807.00888 [hep-th].
- [25] M. Czerny and F. Takahashi, Phys. Lett. B **733**, 241 (2014) doi:10.1016/j.physletb.2014.04.039 [arXiv:1401.5212 [hep-ph]].
- [26] M. Czerny, T. Higaki and F. Takahashi, JHEP **1405**, 144 (2014) doi:10.1007/JHEP05(2014)144 [arXiv:1403.0410 [hep-ph]].
- [27] R. Kallosh and A. Linde, JCAP **1307**, 002 (2013) doi:10.1088/1475-7516/2013/07/002 [arXiv:1306.5220 [hep-th]].
- [28] R. Kallosh, A. Linde and D. Roest, JHEP **1311**, 198 (2013) doi:10.1007/JHEP11(2013)198 [arXiv:1311.0472 [hep-th]].
- [29] R. Kallosh, A. Linde and D. Roest, Phys. Rev. Lett. **112**, no. 1, 011303 (2014) doi:10.1103/PhysRevLett.112.011303 [arXiv:1310.3950 [hep-th]].
- [30] S. Ferrara, R. Kallosh, A. Linde and M. Porrati, Phys. Rev. D **88**, no. 8, 085038 (2013) doi:10.1103/PhysRevD.88.085038 [arXiv:1307.7696 [hep-th]].

- [31] K. D. Lozanov and M. A. Amin, arXiv:1710.06851 [astro-ph.CO].
- [32] U. H. Zhang and T. Chiueh, Phys. Rev. D **96**, no. 2, 023507 (2017) doi:10.1103/PhysRevD.96.023507 [arXiv:1702.07065 [astro-ph.CO]].
- [33] U. H. Zhang and T. Chiueh, Phys. Rev. D **96**, no. 6, 063522 (2017) doi:10.1103/PhysRevD.96.063522 [arXiv:1705.01439 [astro-ph.CO]].
- [34] G. N. Felder, J. Garcia-Bellido, P. B. Greene, L. Kofman, A. D. Linde and I. Tkachev, Phys. Rev. Lett. **87**, 011601 (2001) doi:10.1103/PhysRevLett.87.011601 [hep-ph/0012142].
- [35] S. Antusch, D. Nolde and S. Orani, JCAP **1506**, no. 06, 009 (2015) doi:10.1088/1475-7516/2015/06/009 [arXiv:1503.06075 [hep-ph]].
- [36] P. Brax, J. F. Dufaux and S. Mariadassou, Phys. Rev. D **83**, 103510 (2011) doi:10.1103/PhysRevD.83.103510 [arXiv:1012.4656 [hep-th]].
- [37] R. Micha and I. I. Tkachev, Phys. Rev. Lett. **90**, 121301 (2003) doi:10.1103/PhysRevLett.90.121301 [hep-ph/0210202].
- [38] R. Micha and I. I. Tkachev, Phys. Rev. D **70**, 043538 (2004) doi:10.1103/PhysRevD.70.043538 [hep-ph/0403101].
- [39] S. Kasuya, M. Kawasaki and F. Takahashi, Phys. Lett. B **559**, 99 (2003), M. A. Amin and D. Shirokoff, Phys. Rev. D **81**, 085045 (2010). M. A. Amin, R. Easther, H. Finkel, R. Flauger and M. P. Hertzberg, Phys. Rev. Lett. **108**, 241302 (2012). M. A. Amin, M. P. Hertzberg, D. I. Kaiser and J. Karouby, Int. J. Mod. Phys. D **24**, 1530003 (2014).
- [40] S. Y. Zhou, E. J. Copeland, R. Easther, H. Finkel, Z. G. Mou and P. M. Saffin, JHEP **1310**, 026 (2013)
- [41] S. Antusch, F. Cefala and S. Orani, Phys. Rev. Lett. **118**, no. 1, 011303 (2017)
- [42] S. Antusch, F. Cefala, S. Krippendorff, F. Muia, S. Orani and F. Quevedo, arXiv:1708.08922 [hep-th].
- [43] S. Antusch, F. Cefala and S. Orani, arXiv:1712.03231 [astro-ph.CO].
- [44] M. A. Amin, J. Braden, E. J. Copeland, J. T. Giblin, C. Solorio, Z. J. Weiner and S. Y. Zhou, arXiv:1803.08047 [astro-ph.CO].
- [45] P. A. R. Ade *et al.* [Planck Collaboration], Astron. Astrophys. **594**, A13 (2016) doi:10.1051/0004-6361/201525830 [arXiv:1502.01589 [astro-ph.CO]].
- [46] D. J. E. Marsh, Phys. Rept. **643**, 1 (2016). L. Hui, J. P. Ostriker, S. Tremaine and E. Witten, Phys. Rev. D **95**, no. 4, 043541 (2017).
- [47] P. Agrawal, J. Fan, M. Reece and L. T. Wang, JHEP **1802**, 006 (2018) doi:10.1007/JHEP02(2018)006 [arXiv:1709.06085 [hep-ph]].
- [48] R. Daido, F. Takahashi and N. Yokozaki, Phys. Lett. B **780**, 538 (2018) doi:10.1016/j.physletb.2018.03.039 [arXiv:1801.10344 [hep-ph]].
- [49] P. Agrawal, G. Marques-Tavares and W. Xue, JHEP **1803**, 049 (2018) doi:10.1007/JHEP03(2018)049 [arXiv:1708.05008 [hep-ph]].
- [50] N. Kitajima, T. Sekiguchi and F. Takahashi, Phys. Lett. B **781**, 684 (2018) doi:10.1016/j.physletb.2018.04.024 [arXiv:1711.06590 [hep-ph]].
- [51] P. Adshead, J. T. Giblin and Z. J. Weiner, arXiv:1805.04550 [astro-ph.CO].
- [52] N. Kitajima, J. Soda and Y. Urakawa in preparation.